RSC Advances

PAPER

View Article Online
View Journal | View Issue

Cite this: *RSC Adv.*, 2024, **14**, 16696

Preparation of anisotropic AgNWs/PVA/Ag_2S nanocomposites *via* a vapor-phase sulfidation process

Mahammad Baghir Baghirov, *[a] Mustafa Muradov,[ab] Goncha Eyvazova,[a] Sevinj Mammadyarova, [a] Yashar Azizian-Kalandaragh,[cd] Nahida Musayeva, [e] Gasimov Eldar Kochari[f] and Rzayev Fuad Huseynali [g]

This study used a modified polyol technique to synthesize silver nanowires (AgNWs), which were subsequently mixed with polyvinyl alcohol (PVA) polymer and air-dried under ambient conditions. As a result, AgNWs/PVA nanocomposites with a concentration of 2% were prepared by a casting process. After that, the upper surface of the produced samples was treated with H_2S gas, as a result of which asymmetric structures were formed depending on the gas concentration, exposure time and penetration into the layers. The structural, morphological, and optical properties of these asymmetric structures were analyzed. Changes in the sample structure were studied using X-ray diffraction (XRD), their optical properties were studied using ultraviolet-visible (UV-Vis), Raman spectroscopy, and their morphology using Transmission electron microscopy (TEM). A simple technique involving H_2S gas was used for the sulfidation process of the samples, marking the first exposure of AgNW/PVA nanocomposites to such treatment. Examination of the structural and optical properties of the surfaces revealed clear differences in their physical properties after sulfidation. These obtained results were also supported by TEM images. Finally, the successful production of AgNWs/PVA/Ag_2S anisotropic structure was achieved by this method.

Received 29th February 2024
Accepted 23rd April 2024

DOI: 10.1039/d4ra01585a

rsc.li/rsc-advances

1 Introduction

Composite materials are of particular interest in terms of their flexible and controllable properties. One of these types of composites is AgNWs/PVA nanocomposites. AgNWs have high electrical conductivity, high optical transparency in the visible range.[1] AgNWs have a wide range of applications in solar cells,[2–4] pressure, temperature, and voltage sensors,[5–7] as well as in air purification filters.[8] However, studies show that various difficulties can be experienced during the application of AgNWs. Thus, AgNWs have high chemical activity and can be easily oxidized. Also, the number of contact points of these wires can cause a decrease in conductivity.[9,10] These difficulties can be solved by coating AgNWs. Thus, the use of AgNWs as fillers for the preparation of AgNWs conductive polymer nanocomposites retains the advantages of high surface area and high electrical conductivity, while compensating for the disadvantages of AgNWs.[11,12] One of the polymer materials that can be used in this regard is PVA. Thus, PVA has many applications in terms of its biocompatibility, high dielectric properties, transparency, and easy solubility in water.[13–17] Also, studies show that the sheet resistance and optical transmittance of AgNWs/PVA nanocomposites can be changed by controlling the distribution density of AgNWs within the composite.[18,19]

Ag_2S/PVA nanocomposites are interesting composites. As is known, Ag_2S is a semiconductor with unique physical properties. Thus, Ag_2S has low toxicity, exhibits non-linear optical properties, and exhibits high chemical stability.[20–22] The band gap value varies between 0.9–1.1 eV.[23] Especially high absorption in the NIR region shows that solar cells are widely used in IR detectors.[24] Aziz S. B. *et al.* found that the absorption edge value can be reduced from 5 eV to 1.15 eV by adding Ag_2S to the PVA matrix.[25] Sadovnikov SI. *et al.* found that depending on the size of Ag_2S, the band gap value of Ag_2S/PVA film can be 2.96–2.73 eV.[26] In Ag_2S/PVA nanocomposites, it is observed that the DC electrical conductivity increases with the increase in the amount of filler, which allows the use of these compounds in optoelectronic devices.[24]

Asymmetric structures have recently attracted interest in terms of their field of application. So, these asymmetric

[a]*Nano Research Laboratory, Baku State University, 23 Academic Zahid Khalilov Street, Baku AZ1148, Azerbaijan. E-mail: bmbaghir@gmail.com*
[b]*Analitik LLC, B.Vahabzade 20A, AZ1065, Baku, Azerbaijan*
[c]*Photonics Application and Research Center, Gazi University, 06500 Ankara, Turkey*
[d]*Photonics Department, Applied Science Faculty, Gazi University, 06500 Ankara, Turkey*
[e]*Institute of Physics, Azerbaijan Ministry of Science and Education, H. Javid Ave, 131, AZ1143 Baku, Azerbaijan*
[f]*Department of Cytology, Embryology and Histology, Azerbaijan Medical University. Nasimi Reg., S.Vurgun St., 163, Baku AZ1078, Azerbaijan*
[g]*Electron Microscopy Department, Scientific Research Center, Azerbaijan Medical University, Nasimi Reg., S.Vurgun St., 163, Baku AZ1078, Azerbaijan*

structures are widely used, especially in the field of optical waveguide.[27] Ag nanomaterials are widely used in creating this type of asymmetric structure. These asymmetric structures can be used to create nanowire electrodes for triboelectric nanogenerators (TENGs) and supercapacitors.[28–31] On the other hand, it is known that sulfidation of Ag is carried out both in a liquid environment and under the influence of H_2S gas.[32] Exposing samples to H_2S gas has certain advantages, one of which is to sulfidate the sample from one direction (one side). This, in turn, leads to the acquisition of asymmetric structures. Thus, in this sample, which shows different properties depending on the direction, sulfidation will depend on the concentration of H_2S gas and the diffusion of H_2S gas in the layer. As the gas concentration and sulfidation time increase, the thickness of the sulfidated layer will increase. This in turn will result in an asymmetric structure with respect to the thickness, which will lead to the observation of different physical properties for the sulfided layer. So, this methodology will allow us to create asymmetric structures, and the asymmetry characteristic of this asymmetric structure will depend on the duration and intensity of sulfidation.

In this work, 2wt% AgNWs/PVA thin films were prepared by solution casting method. Then one surface of these films was exposed to H_2S gas. Thus, nanocomposites with anisotropic properties were prepared. Structural and optical properties of sulfidized and non-sulfided surfaces of these nanocomposites were studied.

2 Materials and method

2.1 Synthesis of AgNWs

Silver nanowires were synthesized using a modified polyol method inspired by the literature.[33] Ethylene glycol (EG) was used as both a solvent and a silver-reducing agent, while polyvinylpyrrolidone (PVP, molecular weight: 360 000) acted as a capping agent. Sodium chloride (NaCl) and potassium bromide ($CuBr_2$) were used to maintain charge balance and facilitate growth. In a brief summary of the synthesis process, PVP was dissolved in EG at a concentration of 295.6 mM for 3 hours at an elevated temperature, then was cooled down to room temperature. Solutions of $CuBr_2$ (3.2 mM) and NaCl (15.7 mM) in EG were prepared for later use. Silver nitrate ($AgNO_3$) was dissolved in EG to reach a concentration of 187.8 mM. The synthesis procedure involved placing 5 ml of EG into a 20 ml vial, which was then heated in a silicone oil bath at 160 °C. $CuBr_2$ (100 μl) and NaCl (150 μl) solutions were injected into the vial after 10 minutes. Over the course of 15 minutes, 1.5 ml of $AgNO_3$ and 1.5 ml of PVP solutions were added drop by drop. After the addition of $AgNO_3$ and PVP. The reaction continued for 1.5 hours and was cooled down to room temperature. To collect the silver nanowires, acetone was added to the reaction solution, resulting in precipitates. The precipitates were collected after centrifugation at 4000 rpm for 8 minutes. The washing process was repeated twice to remove excess chemicals. The final product was dispersed in ethanol for future use.

2.2 Preparation and sulfidation process of AgNWs/PVA

AgNWs/PVA were fabricated by operative method. First, PVA is dissolved in water to prepare a 7.5% solution. AgNW was then added to this solution at a concentration of 2 wt%. The mixture was then sonicated for 3 min. The homogeneously mixed solution is filtered into Petri dishes. After filtering, it is air-dried at room temperature for 7 days. Prepared 4 AgNWs/PVA thin films at the same concentration (2wt% AgNWs).

Prepared samples were exposed to H_2S gas. First, 4, 6, 8 g of Na_2S were added to 3 containers (Fig. 1a). Then, these laboratory dishes were coated with AgNWs/PVA nanocomposites (Fig. 1c). Then, 20 ml of HCl solution is added drop by drop to the labware over 30 minutes (Fig. 1d). At this time, according to reaction (1), H_2S was formed in the laboratory container. The sample container was kept for 1 hour. At this time, one side of the composites (towards the inside of the container) was exposed to HCl gas as shown in Fig. 1. That side is conventionally called the bottom side. Thus, AgNWs/PVA/Ag_2S anisotropic structures are formed (Fig. 1e).

$$Na_2S + HCl \rightarrow NaCl + H_2S\uparrow \quad (1)$$

These samples were named AgNWs/PVA+4, AgNWs/PVA+6, AgNWs/PVA+8, according to the Na_2S product used in H_2S production.

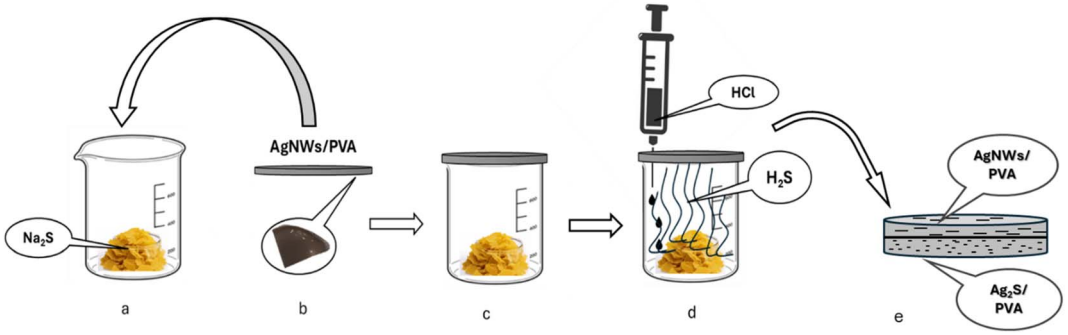

Fig. 1 Sulphidation process of AgNWs/PVA nanocomposites.

2.3 Characterization

The samples underwent structural analysis with the Rigaku Mini Flex 600 X-ray diffractometer (with $\lambda = 1.5406$ Å), utilizing Cu Kα radiation filtered through nickel. Optical characteristics were examined using a Specord 250 Plus UV-Vis Spectrophotometer, spanning wavelengths from 190 to 1100 nm. Raman spectroscopy data were gathered using an EnSpectr R532 spectrometer. Nanoparticles examples were examined under the Transmission Electron Microscope JEM-1400 (JEOL, Japan) at a voltage of 80–120 kV. The morphometric analysis (Min, Max, mean ± SD, *et al.*) of the electronograms was carried out in TIF format *via* a computer program (TEM Imaging Platform-ITEM) developed by Olympus Soft Imaging Solutions GmbH (Germany).

3 Results and discussion

3.1 Structural analysis

The structural examination of AgNWs/PVA thin films is depicted in Fig. 2. From the illustration, it is evident that the spectrum exhibits five distinct peaks. Notably, a well-defined peak with an index of (101) situated at $2\theta = 19.50°$ is indicative of PVA (JCPDS 36-1451).[34] Additionally, peaks corresponding to the (111), (200), (220), and (311) planes, observed at $2\theta = 38.69°$, 45.01°, 65.02°, and 77.90°, respectively, are characteristic of AgNWs (JCPDS card no. 04-0783).[35] These spectra confirm the successful synthesis of AgNWs/PVA thin films.

Fig. 3 shows the structural spectra of AgNWs/PVA composites exposed to H_2S gas. The first spectrum (Fig. 3a) corresponds to the initial AgNWs/PVA composite. Fig. 3b displays the XRD spectrum for the AgNWs/PVA+4 sample. As can be seen from the spectrum, a new peak with (112) index $2\theta = 32.07°$ is observed. This peak is characteristic of Ag_2S formed by sulfidation of the surface of AgNWs under the influence of H_2S gas (JCPDS card no. 14-0072). Fig. 3c and d spectra refer to AgNWs/PVA+6 and AgNWs/PVA+8 samples, respectively, and it is observed that the intensity of the (112) index peak characteristic of Ag_2S is increased. This is due to the increase in the amount of H_2S gas formed during reaction (1), which causes the samples to be exposed to more H_2S gas and more diffusion of H_2S gas into the nanocomposite. Thus, it results in an increase in the amount of Ag_2S formed in the nanocomposite. However, although the intensity of the main peak for AgNWs is reduced compared to the original sample, the peaks characteristic of AgNWs do not disappear in all spectra, indicating that the AgNWs in the sample are not completely sulfided. However, AgNW decomposition and surface sulphidation are thought to occur on the surface directly contacted by the gas. It is also seen that the half-width of the characteristic peak of PVA increases in the XRD spectra of all samples exposed to H_2S gas. This is due to the occurrence of breaks in the polymer chain of PVA due to the effect of H_2S gas and a decrease in the degree of crystallinity.

XRD spectra of both surfaces of the samples exposed to H_2S gas were recorded. Of these, the XRD spectra for the two surfaces

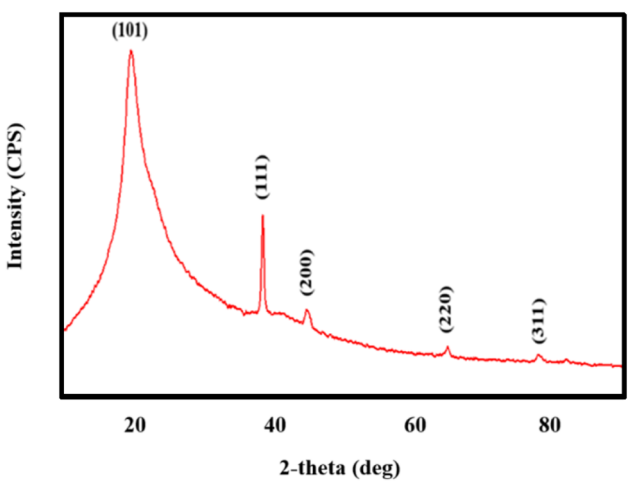

Fig. 2 XRD pattern of AgNWs/PVA nanocomposite.

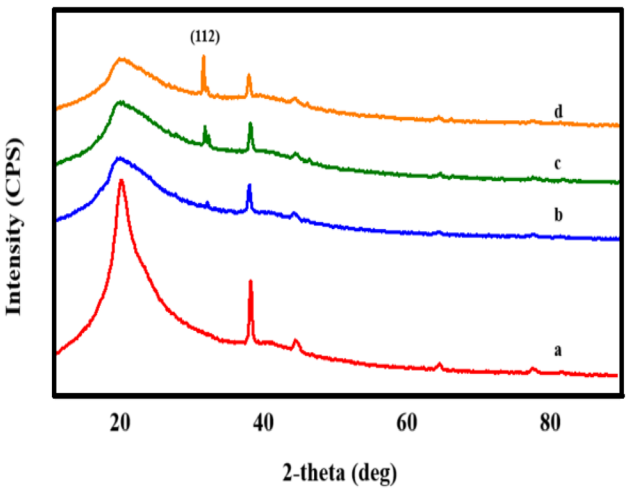

Fig. 3 XRD pattern of (a) AgNWs/PVA, (b) AgNWs/PVA+4, (c) AgNWs/PVA+6, (d) AgNWs/PVA+8.

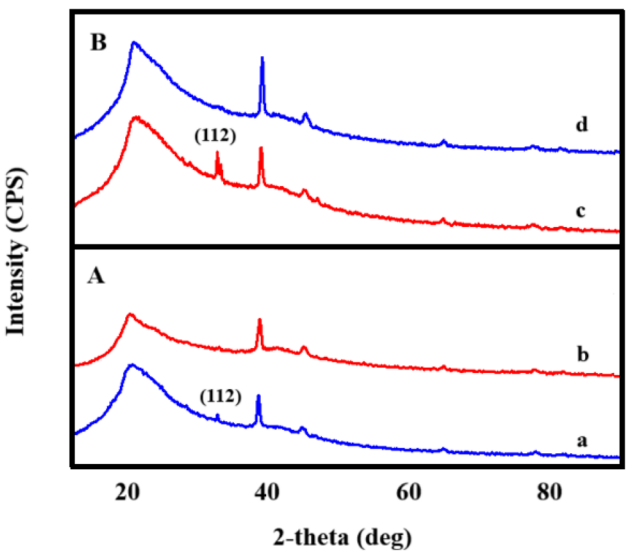

Fig. 4 XRD spectrum of bottom (a) and top (b) surfaces of AgNWs/PVA+4 (A) and AgNWs/PVA+6 (B) samples.

of the AgNWs/PVA+4 sample are shown in Fig. 4A. As can be seen from the spectra, the spectra of the surfaces differ from each other by observing the characteristic peaks of Ag_2S. Thus, although a (112) index peak for Ag_2S is observed in the spectrum obtained from the surface directly exposed to H_2S gas (Fig. 4A(a)), the peak of Ag_2S is not observed on the surface kept in contact with air (Fig. 4A(b)). Ag_2S NWs/PVA- AgNWs/PVA anisotropic structures were obtained by exposure to H_2S gas. Also, Fig. 4B shows the XRD spectra of both surfaces for the AgNWs/PVA+6 sample. As can be seen, the intensity of the (112) peak formed under the influence of H_2S gas increased with the increase of the amount of Na_2S (Fig. 4B(c)). This is due to the fact that the H_2S gas formed by reaction (1) diffuses more into the nanocomposite.

3.2 UV-Vis spectroscopy

Fig. 5A shows the absorption spectra for AgNWs. The absorption spectrum exhibits two relatively sharp surface plasmon resonance peaks at about 350 and 380 nm. The absorption peak at 350 nm could be attributed to the plasmon response of long AgNWs, like that of bulk silver, whereas the peak at 380 nm could be assigned to the transverse plasmon mode of AgNWs.[36] This spectrum demonstrates that AgNWs have been successfully synthesized. Fig. 5B also shows the UV absorption spectra for pure and sulfided AgNWs/PVA nanocomposites. Fig. 5B(a) also shows the absorption spectra for the initial sample, AgNWs/PVA. As can be seen, both peaks characteristic of AgNWs are sharply observed. As can be seen from Fig. 5(b)–(d), when the samples are exposed to H_2S gas, the intensity of the peak associated with these surface plasmons decreases. This is due to the effect of H_2S gas on the surface of Ag nanowires with Ag_2S, disintegration and reduction of plasmon oscillations characteristic of AgNWs. However, considering that all the wires inside the nanocomposite did not react with H_2S and did not sulphide. As a result, the peaks have not completely disappeared.

In addition, due to the effect of H_2S gas, red shifts are observed in the plasmon peaks of the samples (Fig. 5B). The frequency of plasmon peaks depends on the concentration of free electrons (formula (2)).[37] It is known that the red shift of the wavelength leads to a decrease in frequency. This is due to the decrease in the concentration of electrons. Thus, under the influence of H_2S gas, Ag_2S semiconductor is formed on metal AgNWs, which can naturally be associated with a decrease in electron concentration compared to the original sample.

$$\omega = \sqrt{\frac{n_e e^2}{\varepsilon_0 m^*}} \quad (2)$$

ω is the plasmon resonance frequency, n is the density of free electrons, e is the elementary charge, ε_0 is the vacuum permittivity, m^* is the effective mass of the charge carriers.

3.3 Raman spectroscopy

Fig. 6A shows the Raman spectroscopy results for pure PVA. The most intense band centered at 2916 cm^{-1} corresponds to the stretching vibrations of CH_2 in pure PVA. The low intensity peak at 2716 cm^{-1} can be attributed to CH stretching.[38] The peak at 1719 cm^{-1} is due to the stretching of C=O bonds in the PVA structure. The other peaks at 1440 cm^{-1} and 1124 cm^{-1} are attributed to the CH and OH stretching vibrations of PVA molecules. The vibrational mode is defined as a combination of the C–O and C–C stretching modes of PVA at 1124 cm^{-1}. The 852 cm^{-1} and 919 cm^{-1} are associated with C–C vibration.[39,40]

Raman results of AgNWs/PVA nanocomposites have been shown in Fig. 6B. The peak at 237 cm^{-1} is attributed to Ag–N interaction.[41] Two intense peaks at 1360 cm^{-1} and 1582 cm^{-1} are related to C–N and C=O vibrations respectively.[42] The low intensity peak at 2916 cm^{-1} is due to stretching vibrations of CH_2. The Raman spectra of AgNWs/PVA+6 composites are illustrated in Fig. 6C. The Raman spectrum of the AgNWs/PVA+6 sample which is not exposed to H_2S gas (Fig. 6C(a)) exhibits almost the same characteristics as those depicted in Fig. 6B. The Raman spectrum presented in Fig. 5C(b) represents the surface analysis of the AgNWs/PVA+6 nanocomposite exposed to H_2S gas. The intensity of the two distinct peaks

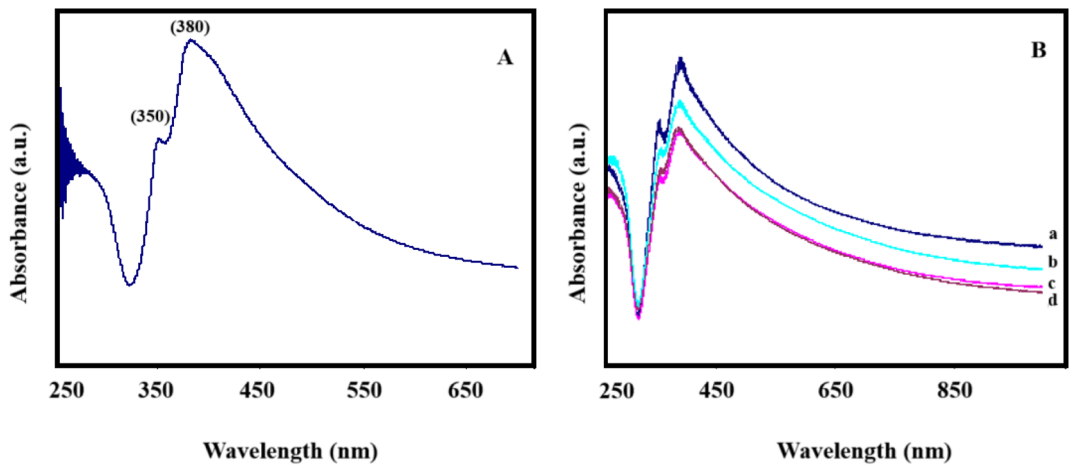

Fig. 5 (A) UV-Vis spectrum for AgNWs. (B) AgNWs/PVA compositions for UV-Vis spectra (a) AgNWs/PVA, (b) AgNWs/PVA+4, (c) AgNWs/PVA+6, (d) AgNWs/PVA+8.

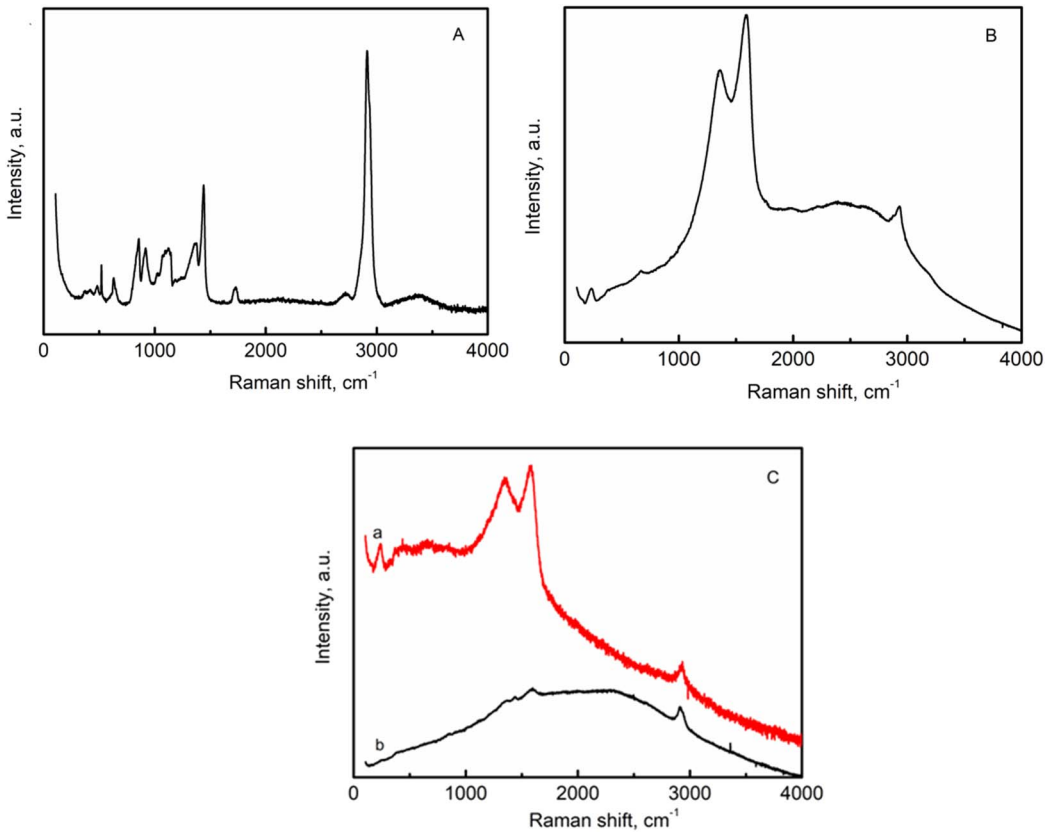

Fig. 6 Raman spectra of (A)-pure PVA; (B) AgNWs/PVA+6; (C) AgNWs/PVA+6 (a) surface not exposed to H_2S gas, (b) surface exposed to H_2S gas).

observed in the sample decreased under the influence of H_2S gas, indicating a deviation in surface properties compared to other surfaces. These results demonstrate the successful formation of the anisotropic structure of AgNWs/PVA-Ag_2S/PVA in the presence of H_2S gas.

3.4 TEM analysis

TEM images displaying silver nanowires synthesized using the modified polyol method are showcased in Fig. 7. The images reveal a variety of lengths and shapes among the AgNWs. The lengths of the AgNWs range between 1.10 and 3.44 μm, demonstrating considerable variation. In contrast, the diameter of these wires appears more consistent, averaging at 60 nm. Furthermore, Fig. 7 illustrates the presence of not just silver nanowires but also particles produced during the synthesis. These particles exhibit an average diameter of approximately 130 nm.

Fig. 8 presents TEM images depicting sulfidized AgNWs/PVA+6 nanocomposites. In Fig. 8A and B, TEM images reveal the

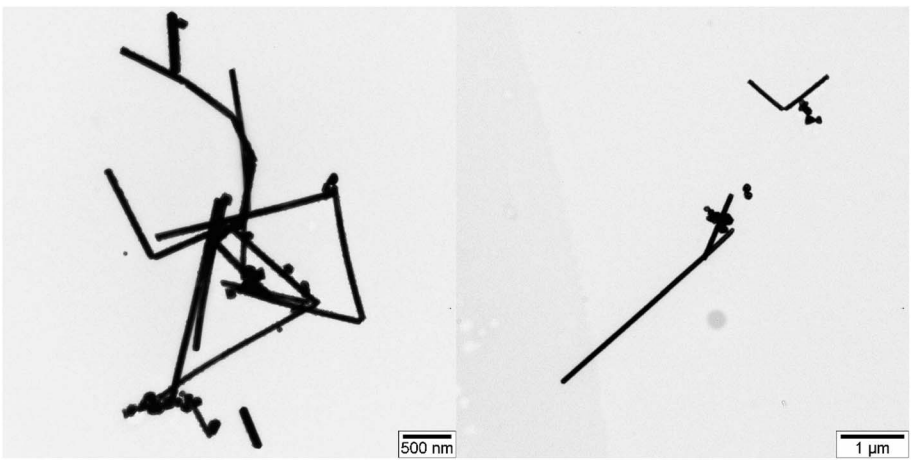

Fig. 7 TEM image for silver nanowires.

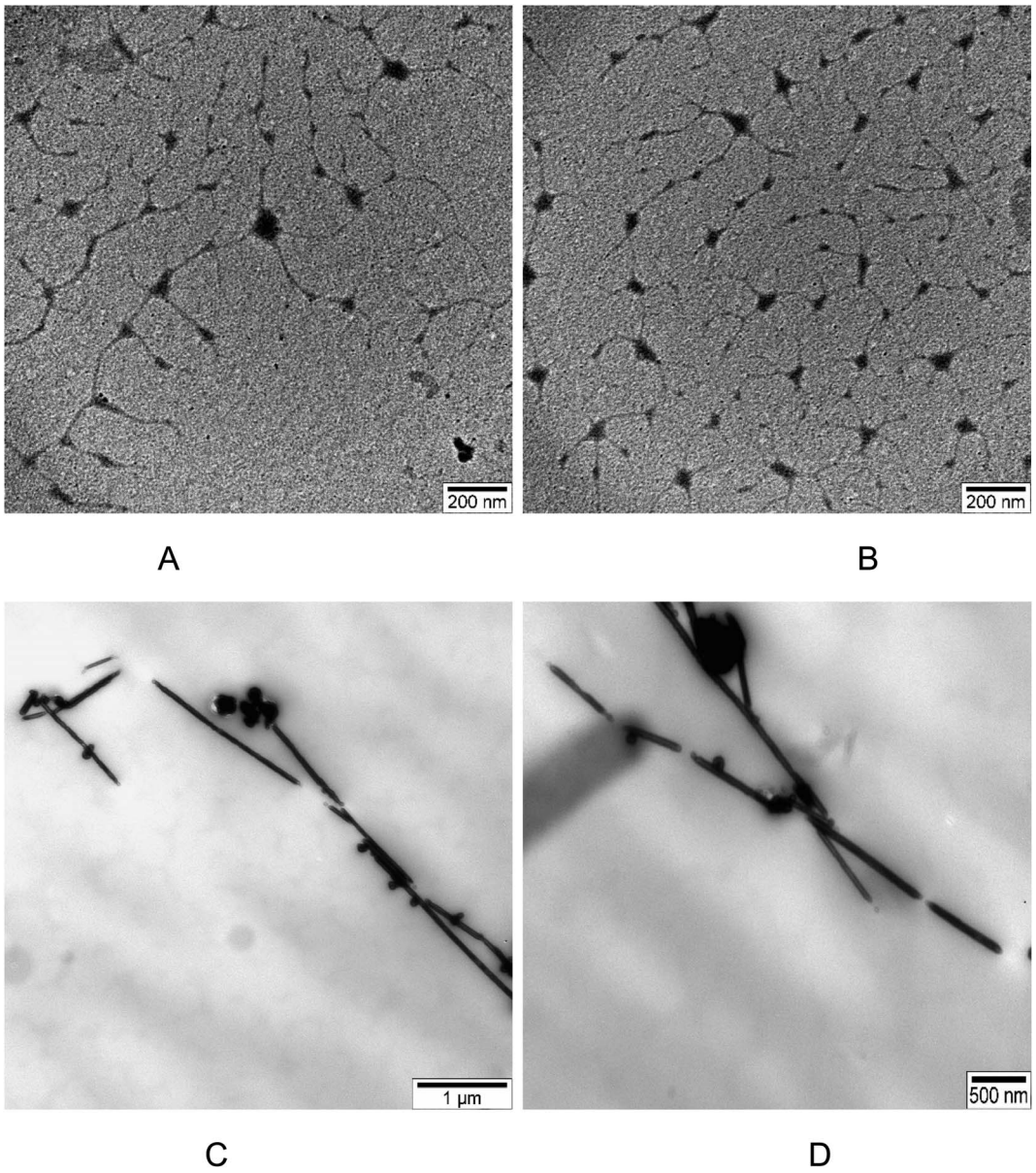

Fig. 8 TEM image for də AgNWs/PVA+6: (A) and (B) bottom of the də AgNWs/PVA+6; (C) and (D) top of the də AgNWs/PVA+6.

sulfided bottom surface. The images vividly display the complete sulfidation and disintegration of silver nanowires due to the influence of H_2S gas. These sulfided Ag_2S particles, fragmented and agglomerated, form centers within the polymer matrix. The diameter of these centers ranges approximately from 70 to 90 nm. Notably, lines are observed between these centers, representing nanoparticles that resist agglomeration during the wire breakdown, with diameters ranging from 20 to 30 nm. Additionally, free particles are evident in Fig. 8, with sizes around 10 nm, identified as Ag_2S particles. Moving on to Fig. 8C and D, they illustrate the non-sulfidation surface of AgNWs/PVA+6 nanocomposites. These images show that the nanowires, akin to their subsurface counterparts, have not entirely disintegrated, retaining their structure to some degree. However, the introduction of a small quantity of H_2S gas into this layer has caused fractures along the length of these nanowires.

4 Conclusion

In this study, silver nanowires were synthesized by modified silver polyol method. Then AgNW/PVA nanocomposites were prepared by incorporating PVA at a concentration of 2 wt%. Then this composite was exposed to H_2S gas in one direction for different periods of time. Then, the properties of both surfaces of the nanocomposite were studied. Structural analysis shows that AgNWs were sulfided and Ag_2S was formed on the surface exposed to H_2S gas. Also, breaks in the polymer chain occurred

and the degree of crystallinity of the polymer decreased. Also, this structural change depends on the exposure time of H_2S gas. Raman analysis confirmed these observations and characteristic peaks for AgNWs/PVA nanocomposites were observed. The intensity of these peaks directly decreased on the surface exposed to H_2S gas. In addition, UV-Vis spectroscopy shows that under the influence of H_2S gas, the intensity of the peaks of the plasmon oscillations of the samples decreases, and the peak shifts to the red. This is due to the decrease in the concentration of free electrons as the wires move to Ag_2S. TEM images confirm that the nanowires in the sample were disintegrated and sulphided by H_2S gas. But it also shows that the wire retains its shape and structure to a certain extent. The aforementioned results confirm that asymmetric structures are successfully prepared with the new methodology.

Conflicts of interest

There are no conflicts to declare.

Acknowledgements

This work was partially supported by Analytic LLC.

References

1 R. F. Hamans, M. Parente, A. Garcia-Etxarri and A. Baldi, *J. Phys. Chem. C*, 2022, **126**(20), 8703–8709.
2 S. Lee, J. Jang, T. Park, Y. M. Park, J. S. Park, Y. K. Kim, H. K. Lee, E. C. Jeon, D. K. Lee, B. Ahn and C. H. Chung, *ACS Appl. Mater. Interfaces*, 2020, **12**(5), 6169–6175.
3 J. Jin, J. Li, Q. Tai, Y. Chen, D. D. Mishra, W. Deng, J. Xin, S. Guo, B. Xiao and X. Wang, *J. Power Sources*, 2021, **482**, 228953.
4 C. Xie, C. Xiao, J. Fang, C. Zhao and W. Li, *Nano Energy*, 2023, **107**, 108153.
5 S. Yao and Y. Zhu, *Nanoscale*, 2014, **6**, 2345–2352, DOI: 10.1039/c3nr05496a.
6 J. Wang, J. Jiu, M. Nogi, T. Sugahara, S. Nagao, H. Koga, P. He and K. A. Suganuma, *Nanoscale*, 2015, **7**, 2926–2932, DOI: 10.1039/C4NR06494A.
7 W. Hu, X. Niu, R. Zhao and Q. Pei, *Appl. Phys. Lett.*, 2013, **102**, 083303, DOI: 10.1063/1.4794143.
8 M. Ma, D. Du, C. Yu, J. Wang and Z. Wang, *Appl. Surf. Sci.*, 2024, **644**, 158814.
9 C. T. Chou and F. H. Wang, *J. Vac. Sci. Technol., A*, 2018, **36**(5), 05G504.
10 F. Duan, W. Li, G. Wang, C. Weng, H. Jin, H. Zhang and Z. Zhang, *Nano Res.*, 2019, **12**, 1571–1577.
11 N. M. Abbasi, H. Yu, L. Wang, Z. U. Abdin, W. Amer, M. Akram, H. Khalid, Y. Chen, M. Saleem, R. Sun, *et al.*, *Mater. Chem. Phys.*, 2015, **166**, 1–15.
12 Y. Sun, X. Wang and H. Zhang, *Biosensors*, 2022, **12**(6), 382.
13 M. Muradov, M. B. Baghirov, G. Eyvazova, L. Gahramanli, S. Mammadyarova, G. Aliyeva, E. Huseynov and M. Abdullayev, *Radiat. Phys. Chem.*, 2023, **208**, 110926.
14 X. Wu, Y. Xie, C. Xue, K. Chen, X. Yang, L. Xu, *et al.*, *Mater. Res. Express*, 2019, **6**(7), 075306.
15 L. Badrinezhad, C. Bilkan, Y. Azizian-Kalandaragh, A. Nematollahzadeh, I. Orak and S. Altindal, *Int. J. Mod. Phys. B*, 2018, **32**, 175027.
16 O. Azhar, Z. Jahan, F. Sher, M. B. Niazi, S. J. Kakar and M. Shahid, *Mater. Sci. Eng. C*, 2021, **126**, 112127.
17 L. Gahramanli, M. Muradov, G. Eyvazova, M. B. Baghirov, S. Mammadyarova, G. Aliyeva, E. Hajiyev, F. Mammadov and S. Bellucci, *Chem. Eng.*, 2023, **7**(5), 92.
18 W. Lan, Y. Chen, Z. Yang, W. Han, J. Zhou, Y. Zhang, J. Wang, G. Tang, Y. Wei, W. Dou and Q. Su, *ACS Appl. Mater. Interfaces*, 2017, **9**(7), 6644–6651.
19 K. Yadav, R. Nain, M. Jassal and A. K. Agrawal, *Compos. Sci. Technol.*, 2019, **182**, 107766.
20 J. Feng, X. Li, Z. Shi, C. Zheng, X. Li, D. Leng, Y. Wang, J. Liu and L. Zhu, *Adv. Opt. Mater.*, 2020, **8**(6), 1901762.
21 C. Ding, Y. Huang, Z. Shen and X. Chen, *Adv. Mater.*, 2021, **33**(32), 2007768.
22 A. Badawi and S. S. Alharthi, *Mater. Sci. Semicond. Process.*, 2020, **116**, 105139.
23 C. Du, J. Tian and X. Liu, *Mater. Chem. Phys.*, 2020, **249**, 122961.
24 S. S. Alharthi, A. Alzahrani, M. A. Razvi, A. Badawi and M. G. Althobaiti, *J. Inorg. Organomet. Polym. Mater.*, 2020, **30**, 3878–3885.
25 S. B. Aziz, M. A. Rasheed, A. M. Hussein and H. M. Ahmed, *Mater. Sci. Semicond. Process.*, 2017, **71**, 197–203.
26 S. I. Sadovnikov, A. V. Ishchenko and I. A. Weinstein, *Mater. Sci. Eng. B*, 2023, **296**, 116667.
27 S. P. Abbasi and A. Hodaei, *Int. j. opt. photonics*, 2021, **15**(2), 125–132.
28 Y. Mao, J. Xie, H. Liu and W. Hu, *Chem. Eng. J.*, 2021, **405**, 126984.
29 Y. Mao, Y. Li, J. Xie, H. Liu, C. Guo and W. Hu, *Nano Energy*, 2021, **84**, 105918.
30 Y. Li, J. Zhu, J. Xie, Y. Mao and W. Hu, *J. Colloid Interface Sci.*, 2023, **650**, 1113–1124.
31 Y. Mao, J. Xie, C. Guo, H. Liu, H. Xiao and W. Hu, *Chem. Eng. J.*, 2021, **426**, 131188.
32 M. B. Baghirov, M. Muradov, G. Eyvazova, Y. Azizian-Kalandaragh, S. Mammadyarova, J. Kim, E. Gasımov and F. Rzayev, *RSC Adv.*, 2024, **14**(4), 2320–2326.
33 S. Fahad, L. Wang, J. Liu, S. Li, J. Fu, B. U. Amin, R. U. Khan, S. Mehmood, F. Haq, W. Nan and M. Usman, *Mater. Chem. Phys.*, 2021, **267**, 124643.
34 R. Kandulna and R. B. Choudhary, *Polym. Bull.*, 2018, **75**, 3089–3107.
35 J. Lu, D. Liu and J. Dai, *J. Mater. Sci.: Mater. Electron.*, 2019, **30**(16), 15786–15794.
36 A. Comin and L. Manna, *Chem. Soc. Rev.*, 2014, **43**(11), 3957–3975.
37 M. B. Gebeyehu, T. F. Chala, S. Y. Chang, C. M. Wu and J. Y. Lee, *RSC Adv.*, 2017, **7**(26), 16139–16148.
38 F. Barzegar, A. Bello, M. Fabiane, S. Khamlich, D. Momodu, F. Taghizadeh, J. Dangbegnon and N. Manyala, *J. Phys. Chem. Solids*, 2015, **77**, 139–145.

39 N. A. Zubair, N. A. Rahman, H. N. Lim, R. M. Zawawi and Y. Sulaiman, *RSC Adv.*, 2016, **6**(21), 17720–17727.
40 Y. Kan, J. V. Bondareva, E. S. Statnik, J. Cvjetinovic, S. Lipovskikh, A. S. Abdurashitov, M. A. Kirsanova, G. B. Sukhorukhov, S. A. Evlashin, A. I. Salimon and A. M. Korsunsky, *Nanomaterials*, 2022, **12**(6), 998.
41 M. Chen, H. Zhang, Y. Ge, S. Yang, P. Wang and Y. Fang, *Langmuir*, 2018, **34**(50), 15160–15165.
42 B. Heidari, S. Salmani, M. Sasani Ghamsari, M. Ahmadi and M. H. Majles-Ara, *Opt. Quantum Electron.*, 2020, **52**, 1–18.